

Toward efficient and tailorable mid-infrared emitters utilizing multilayer graphene

Cite as: Appl. Phys. Lett. **120**, 051105 (2022); <https://doi.org/10.1063/5.0079777>

Submitted: 08 December 2021 • Accepted: 19 January 2022 • Published Online: 01 February 2022

Prarthana Gowda,  Dean A. Patient, Simon A. R. Horsley, et al.



View Online



Export Citation



CrossMark

ARTICLES YOU MAY BE INTERESTED IN

[Tailoring the spectral properties of layered chiral mid-infrared metamaterials](#)
Applied Physics Letters **119**, 241102 (2021); <https://doi.org/10.1063/5.0066386>

[Mid-infrared type-II InAs/InAsSb quantum wells integrated on silicon](#)
Applied Physics Letters **117**, 131103 (2020); <https://doi.org/10.1063/5.0022235>

 QBLOX



1 qubit

Shorten Setup Time

Auto-Calibration
More Qubits

Fully-integrated

Quantum Control Stacks
Ultrastable DC to 18.5 GHz
Synchronized <<1 ns
Ultralow noise



100s qubits

[visit our website >](#)



Toward efficient and tailorable mid-infrared emitters utilizing multilayer graphene

Cite as: Appl. Phys. Lett. **120**, 051105 (2022); doi: [10.1063/5.0079777](https://doi.org/10.1063/5.0079777)

Submitted: 8 December 2021 · Accepted: 19 January 2022 ·

Published Online: 1 February 2022




View Online



Export Citation



CrossMark

Prarthana Gowda, Dean A. Patient,  Simon A. R. Horsley, and Geoffrey R. Nash ^{a)} 

AFFILIATIONS

College of Engineering, Mathematics and Physical Sciences, University of Exeter, Exeter EX4 4QF, United Kingdom

^{a)} Author to whom correspondence should be addressed: g.r.nash@exeter.ac.uk

ABSTRACT

There is a continuing need for the development of cost-effective and sustainable mid-infrared light sources for applications such as gas sensing and infrared beacons. A natural replacement for the conventional incandescent sources still widely used in such applications is semiconductor LEDs, but to achieve emission at long wavelengths requires the realization of devices with narrow effective bandgaps, inherently leading to relatively poor internal and external quantum efficiencies. Recently, the technological potential of graphene-based incandescent emitters has been recognized, in part due to the ability of graphene to sustain extremely large current densities. Here, we introduce a simple architecture, consisting of a back-reflector behind a multilayer graphene filament, which we use to produce emitters with wall-plug-efficiencies comparable to state-of-the-art semiconductor cascade LEDs. Coupled with the potential for high-speed modulation, resulting from the low thermal mass, our results demonstrate the feasibility of creating practicable infrared sources.

© 2022 Author(s). All article content, except where otherwise noted, is licensed under a Creative Commons Attribution (CC BY) license (<http://creativecommons.org/licenses/by/4.0/>). <https://doi.org/10.1063/5.0079777>

Over the last few decades, advances in semiconductor optoelectronics have revolutionized areas such as communications, sensing, and consumer electronics. One important example of this is the need for efficient cost-effective, sustainable mid-infrared (mid-IR) components, covering the 2–12 μm wavelength range for applications such as gas sensing and IR beacons. A natural replacement for the conventional incandescent sources still widely used in such applications is semiconductor LEDs,¹ but to achieve emission at relatively long wavelengths requires the realization of devices with narrow effective bandgaps. This inherently leads to relatively poor internal² and external quantum efficiencies.³ Although room-temperature mid-IR semiconductor LEDs were first demonstrated several decades ago, they, therefore, still suffer from relatively low overall efficiencies. For example, the room temperature wall-plug efficiency (WPE), the ratio of the electrical power in to the optical power out, of the $\text{Al}_x\text{In}_{1-x}\text{Sb}$ based LEDs described by Nash *et al.*¹ was approximately 0.02%. Much higher values of WPE can be achieved in interband cascade devices, for example, 0.15% at 3.3 μm ,⁴ but such cascade structures require the precise epitaxial growth of a large number of layers. Mid-IR semiconductor LEDs also typically incorporate elements, such as indium and gallium, raising concerns regarding sustainability.

The performance of incandescent emitters can be improved by miniaturizing them, to increase their modulation speeds, and by

employing nanophotonic techniques to control and enhance emission.^{5–8} Silicon based micro-machined heaters^{9,10} have the advantage of being CMOS compatible but still have a relatively slow response time (maximum modulation frequencies of ~ 100 Hz). Wojszzyk *et al.*¹¹ recently reported an incandescent emitter incorporating a metasurface operating at very high frequencies, up to 20 MHz, but with a value of wall plug efficiency of 10^{-6} at a modulation frequency of 20 KHz, although it was shown that emission decays as a function of the square root of the frequency, so that an efficiency of 0.01% is expected at 2 Hz.

The low thermal mass of graphene, compared even to silicon micro-heaters, coupled with its ability to sustain extremely large current densities, offers an alternative route for the development of high speed advanced incandescent emitters.^{12–22} For example, Miyoshi *et al.*¹⁴ integrated graphene emitters onto silicon chips to demonstrate emission in the near infrared that could be modulated at high frequencies (100-ps response time), although efficiency was not considered. In this manuscript, we demonstrate an infrared light source, incorporating a multilayer graphene (MLG) emitter layer and a Salisbury screen back-reflector with WPEs comparable to state-of-the-art semiconductor cascade LEDs. Ultimately, these sources could be both more cost effective and sustainable to manufacture than compound semiconductor based alternatives.

The behavior of the graphene based emitting devices can be described using two theoretical approaches: an analytic model based on the fluctuation-dissipation theorem (FDT)²³ for a device in non-thermal equilibrium, and the application of Kirchhoff's law of thermal radiation to approximate the device as being in thermal equilibrium. In the latter case, the emissivity is given as the temperature and wavelength dependent absorption of the device.²⁴ Two different types of devices, incorporating MLG (12 layers), as the emitting element, were considered. In the first type of device, the multilayer graphene sits upon a 300 nm thick layer of insulating SiO₂, which in turn sits on a silicon substrate. In the second type of device, a thin back reflector (50 nm thick aluminum) is also incorporated between the silicon substrate and SiO₂, as shown schematically in Fig. 1(a).

We compare two formulas for the average emitted power \hat{S} . We first apply the fluctuation-dissipation theorem (FDT)²³ to a planar multi-layer that has variable temperature T and permittivity ϵ .²⁵ Here, the emitted power is given by

$$\langle \hat{S}(z, \lambda, T) \rangle = \int dz' \frac{128 \hbar \pi^4 c^2}{D^2} \frac{1}{\lambda^8} \left(\frac{1}{\exp\left[\frac{2\pi\hbar c}{\lambda k_B T}\right] - 1} \right) \times \text{Im}[\epsilon(z', \lambda, T)] |G(z, z', \lambda)|^2, \quad (1)$$

where D is the distance between the source and the observer, $\epsilon(z', \lambda, T)$ is the permittivity of the emitting material, and $G(z, z', \lambda)$ is 1D scalar Greens' function. To apply this formula, we assume that all layers emit at an ambient temperature (300 K), except for the multilayer graphene, which has a higher temperature due to Joule heating induced by an applied current.

In the second approach, we approximate the aluminum layer as a perfect electrical conductor and take the SiO₂ layer as lossless in the wavelength range of interest. As emission from each portion of the device scales with the local value of $\text{Im}[\epsilon]$, only the graphene layer contributes to the emission, and we can, thus, take the temperature in Eq. (1) as uniform throughout the device, reducing our theory to Kirchhoff's law of thermal radiation.²⁴ For more details on the relationship between these two theories, see Ref. 26. The whole device is then a greybody with temperature and wavelength dependent emissivity, $\epsilon_I(\lambda, T)$, given as the absorption of the system

$$B(\lambda, T) = \frac{2\pi\hbar c^2}{\lambda^5} \epsilon_I(\lambda, T) \frac{1}{\exp\left[\frac{2\pi\hbar c}{\lambda k_B T}\right] - 1}, \quad (2)$$

where $B(\lambda, T)$ is the emission. We assume that the multilayer graphene consists of randomly stacked layers of graphene with the conductivity of each layer given by²⁷

$$\sigma(\omega, T) = \frac{2e_0^2 k_B T}{\pi \hbar} \frac{i}{\omega + i\Gamma} \log \left[2 \cosh \left(\frac{E_F}{2k_B T} \right) \right] + \frac{e_0^2}{4\hbar} \left[H \left(\frac{\omega}{2} \right) + \frac{4i\omega}{\pi} \int_0^\omega d\epsilon \frac{H(\epsilon) - H \left(\frac{\omega}{2} \right)}{\omega^2 - 4\epsilon^2} \right], \quad (3)$$

where i is the imaginary unit, the frequency $\omega = 2\pi c/\lambda$, E_F is the Fermi energy, and Γ is the plasma decay rate. The first (second) term represents the intra (inter) band contributions to the conductivity. Here, we allow $\Gamma = 1/(1.3 \times 10^{-13})$, and

$$H(\epsilon) = \frac{\sinh \left(\frac{\hbar \epsilon}{k_B T} \right)}{\left(\cosh \left(\frac{E_F}{k_B T} \right) + \cosh \left(\frac{\hbar \epsilon}{k_B T} \right) \right)}. \quad (4)$$

In this way, we can represent the N layers of randomly stacked graphene as one layer of graphene with thickness $N \times 1 \text{ \AA}$. From this, the permittivity is given as

$$\epsilon(\omega, T) = 1 + i \frac{\sigma(\omega, T)}{\epsilon_0 \omega d}, \quad (5)$$

where d is the thickness of a single graphene layer. The Green function and emissivity were both calculated analytically using the transfer matrix method²⁸ with the permittivity of SiO₂ and aluminum taken from Ref. 29. In the calculations, we compare emission from multilayer graphene on a semi-infinite layer of SiO₂ and on a finite SiO₂ layer deposited on aluminum.

To model the emission from the two devices, we assume that in the OFF state (no current applied), the system is at 300 K. A non-linear least squares fitting tool³⁰ was used to fit the emission spectra calculated using Eqs. (1) and (2) to experimentally measured spectra, allowing two quantities to vary: (1) the temperature of the device (the "ON" temperature) and (2) a scaling factor that is a combination of physical constants such as the device area and parameters such as the distance between the emitter and observer. This scaling factor is the same for both devices.

Devices consisting of multilayer graphene (12–14 layers) were fabricated using two different substrates. The first consisted of a silicon

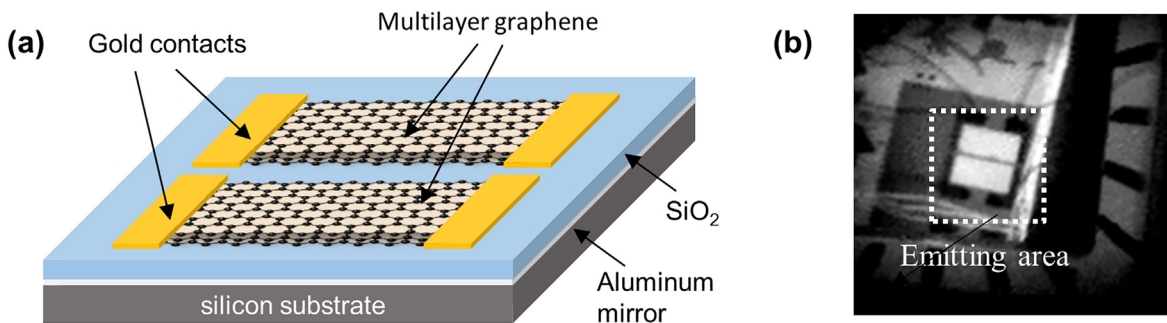


FIG. 1. (a) Schematic diagram of a graphene based emitter containing a back reflector. (b) Infrared image of the device with both segments driven at 1 Hz.

substrate with a 300 nm top layer of SiO₂, whereas the second substrate incorporated a thin back reflector (50 nm thick aluminum) between the silicon substrate and top SiO₂ [Fig. 1(a)]. Multilayer graphene was transferred by graphene supermarket onto the two types of substrates before lithography and dry etching were used to define an emitting area consisting of two 500 $\mu\text{m} \times 1$ mm rectangular segments (with a 50 μm gap between them), which could be driven independently. Gold contacts were realized using 5 nm of Cr and 80 nm of Au.

Finished devices were mounted on ceramic chip holders, and all measurements were performed at ambient temperature and with the devices under vacuum. Two terminal measurements of the device resistances were made at low currents, so that there was minimal heating with typical values obtained of $\sim 800 \Omega$ per segment (or equivalent to $\sim 400 \Omega/\square$). These values are approximately $3\times$ smaller than those reported previously from similar devices containing CVD MLG with three to six layers of graphene,¹⁹ consistent with the decrease in resistance expected from an increased number of graphene layers.²⁷

The spatial characteristics of emission were assessed using a FLIR Systems model A655 long-wavelength infrared imager, and Fig. 1(b) shows the emission from the device containing the back reflector. Both segments of the device were simultaneously driven with a 1 Hz square waveform (50% current) at a peak current of 20 mA. The captured images show that emission from both segments is highly uniform. The spectral characteristics of the devices were assessed by collecting emission using a CaF₂ lens before focusing the light, using a second CaF₂ lens, onto the entrance of a Jobin-Yvon iHR550 spectrometer, equipped with a 4 μm blazed diffraction grating. Light exiting the spectrometer was focused onto a liquid nitrogen cooled HgCdTe detector with a 2–12 μm response, and the signal from the detector was amplified by a low noise preamplifier and passed to a lock-in amplifier for phase sensitive measurement. To correct for the efficiency of the optical system, and absorption by CO₂ and water in the atmosphere, the measurements were calibrated using a 673 K blackbody source. Emission spectra were obtained with one segment of the devices driven with a 1 kHz square waveform (50% current) and at a peak current of 90 mA using a phase sensitive measurement. Device resistances were observed to decrease slightly (by around 25%) relative to the values obtained at low currents, consistent with the conduction being graphene-like, leading to voltages of around 50 V required to drive 90 mA. Results are presented from two devices, but similar behavior was observed from a number of other devices.

The measured emission spectrum from a device without a back-reflector is shown in Fig. 2(a). (Note that absorption by atmospheric water and CO₂ results in residual features in the measured spectra at wavelengths of 3 and 4.2 μm . Features at 3.4 μm are thought to be due to the presence of polymer residues.) Also shown in Fig. 2(a) are two theoretical fits to the measured data based on the non-equilibrium model [Eq. (1)] with values of the Fermi energy E_f of 0 and -0.2 eV. The fits to the measured data using the second theoretical approach, which assumes the device is in thermal equilibrium [Eq. (2)], were identical [and for completeness is shown in supplementary material Fig. 1(a)]. Fits yielded ON temperatures of 642 and 514 K for values of E_f of 0 and -0.2 eV, respectively, consistent with values previously obtained at similar currents in similar devices.²¹ The equivalence of two theoretical approaches in describing emission from the device is because the SiO₂ layer is lossless over this wavelength range and so

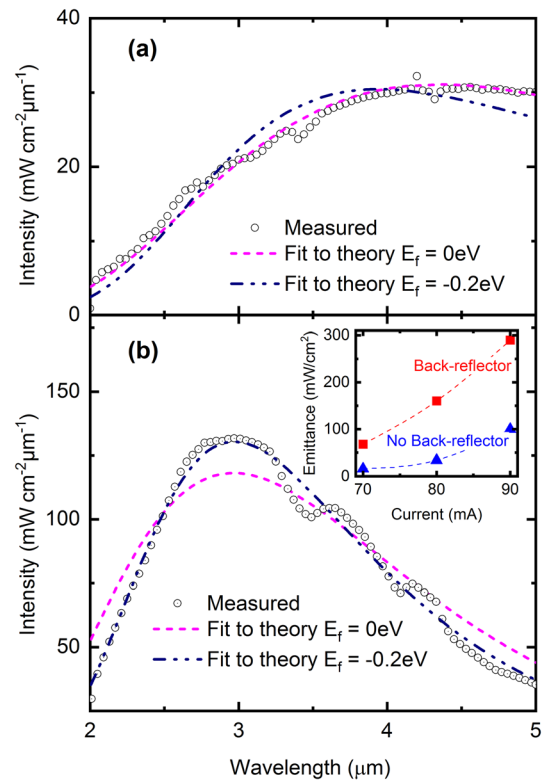


FIG. 2. Measured emission spectrum (gray symbols) together with fits to the data using the non-equilibrium model (lines) for devices (a) without and (b) with back-reflector. In both types of devices, fits to the non-equilibrium and equilibrium models give exactly the same result. The inset shows the measured total integrated emittance as a function of the drive current.

does not contribute to emission as described in Eq. (1). As the multilayer graphene is the only part of the device emitting, the device can also be approximated as being in thermal equilibrium, so that the two theoretical models produce identical results.

In devices incorporating a back-reflector, Fig. 2(b), the measured peak emission shifts to much shorter wavelengths, from approximately from 4.5 to 3 μm , and also increases by a factor of approximately four, from ~ 30 to ~ 140 $\text{mW}/\text{cm}^2/\mu\text{m}$. Theoretical fits to the measured data using the non-equilibrium model [Eq. (1)] are also shown in Fig. 2(b), again for values of E_f of 0 and -0.2 eV. In this case, a better fit to the measured spectrum was achieved using a value of the Fermi energy of -0.2 eV, reflecting the fact that graphene is likely to have significant intrinsic hole doping,¹⁸ although this is hard to characterize experimentally in these samples. As for the device without the back-reflector, both theoretical models give exactly identical results, yielding ON temperatures of 720 and 561 K for values of E_f of 0 and -0.2 eV, respectively. [The fits to the data using Eq. (2) are shown in supplementary material Fig. 2(b).] In this case, the two theoretical approaches are equivalent as the aluminum layer acts a perfect mirror, meaning that there it contributes little to emission, other than serving to reflect the emitted waves to give this larger, shifted emission peak. The total measured integrated emission from the devices without and with the back reflector is plotted as a function of the drive current in

the inset of Fig. 2(b). In both cases, the measured emission increases rapidly as a function of the increasing current, as expected if the measured emission being proportional to T^4 , where T is the temperature of the graphene. Further work is under way to study the evolution of emission over a wider range of input powers.

The significant enhancement in emission observed in the device with a back-reflector is due to the aluminum mirror effectively acting as a Salisbury screen: at a given wavelength, the wave will accrue the phase by reflecting off the back reflector and being absorbed fully by the multilayer graphene, resulting in large emission in that region. In Fig. 3, calculated emission spectra are plotted as a function of the SiO_2 layer thickness for the device with a back-reflector. Here, parameters were taken from the fits ($E_f = 0$ eV) to the measured data shown in Fig. 2. Calculated emission spectra correspond to the difference between two greybodies at temperatures of 720 and 300 K for consistency with the experiments. Changing the thickness serves to shift the wavelength at which the Salisbury screen effect is strongest, changing the peak emission wavelength—where the peak emissivity corresponds to the peak wavelength in emission. These spectra show that there is further scope to increase the device output just by optimizing the position of the back-reflector.

However, even without optimization of the device design, the total measured integrated emission from the devices without and with the back reflector was approximately 100 and 300 mW/cm^2 , respectively,

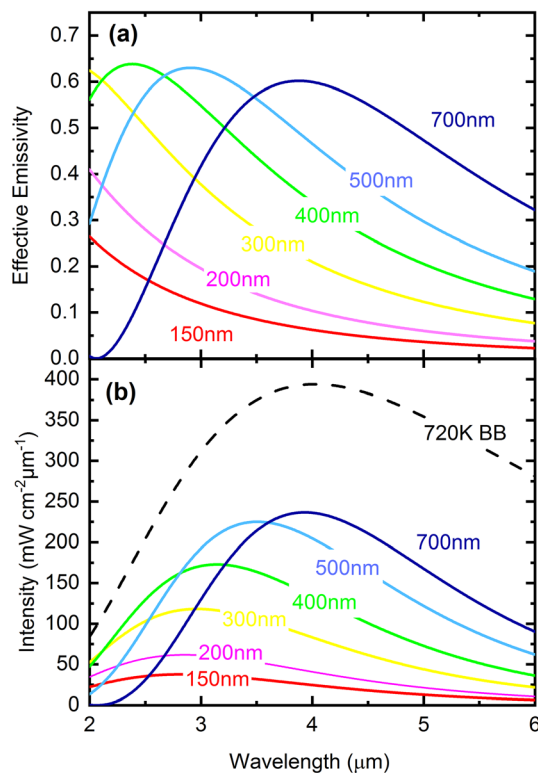


FIG. 3. (a) The calculated effective emissivity and (b) the calculated emission plotted as a function of the thickness of the SiO_2 layer. The yellow lines represent the case, where SiO_2 is the same thickness as in the experiments, and a dashed black line is for a blackbody at a temperature of 720 K.

yielding associated values of wall plug efficiencies of approximately 0.02% and 0.07%. These values compare, for example, to values of 0.1% in superluminescent LEDs operating at $5 \mu\text{m}$ (Ref. 31) or a value of extrinsic efficiency of 0.084% in mechanical exfoliated black phosphorous based LEDs.³² Such high relative efficiencies, therefore, demonstrate the feasibility of developing practicable graphene based mid-infrared light emitting devices which, in contrast to semiconductor LEDs and MEMS equivalents, are relatively simple to fabricate. Further gains in the efficiency could be achieved by optimizing the geometry of the emitting area; for example, Brucoli *et al.*³³ proposed a quasimonochromatic emitter with a circular metallic filament positioned over a gold mirror and showed theoretically that a value of the wall plug efficiency of 6.5% could be achieved in this geometry.

Finally, addition of a back reflector, therefore, serves to improve overall emission and create a broadband emission peak. However, emission from these devices could also be tailored by placing a resonant material, such as a metamaterial consisting of metallic resonators,²² on the multilayer graphene to create an emission spectrum with a strong, narrowband emission peak, which would be advantageous for gas-sensing applications. Here, we model such an additional layer as a 50 nm thick isotropic resonant layer whose permittivity obeys

$$\epsilon(\omega) = 1 + \frac{A(\omega_0^2 - \omega^2)}{(\omega_0^2 - \omega^2) + (\gamma\omega)^2} + i \frac{A\gamma\omega}{(\omega_0^2 - \omega^2) + (\gamma\omega)^2}, \quad (6)$$

where A determines the strength of the resonance, ω_0 , and the line-width is determined by γ . Putting this layer on top of the graphene structure already established should create a strong emission peak at the resonant frequency, resulting in a large emission peak at the same wavelength. Here, we choose that resonance to occur at $4 \mu\text{m}$ with $\gamma = 0.1 \times 10^{14}$ and $A = 10 \times 10e^{28}$, giving a permittivity profile for the resonant layer [Fig. 4(a)] and emission spectra for the whole device (metamaterial, graphene, SiO_2 , Al, Si) [Fig. 4(b)]. As before, parameters were taken from the fits to measured data ($E_f = 0$) shown in Fig. 2, and the calculated spectrum corresponds to the difference between two greybodies at temperatures of 720 and 300 K. The resonant layer acts as free space outside the resonant frequency, leaving the emission spectra that are the same as the normal device with a back reflector; however, at the resonant frequency, the large emissivity peak creates a large narrowband emission peak at the target wavelength, whose peak is close to that of a perfect blackbody.

In conclusion, we have investigated the characteristics of mid-infrared thermal emission from devices containing a multilayer graphene emitting layer with or without a near-field back-reflector. Analytic models were designed using the fluctuation-dissipation theorem, as well as using Kirchhoff's law of thermal radiation, to devise two methods to model these devices: one where each component of the device is not in thermal equilibrium, and the other allows the device to be in thermal equilibrium, where the emissivity of the device (greybody factor) is then given as the absorption of the device. We find that in both cases, both models yield identical results, demonstrating that the wavelength and temperature dependent greybody factor can be used to accurately model the emission from both types of devices.

In devices containing a back-reflector, the measured peak emission increased by a factor of four and also shifted to shorter wavelengths. The total integrated emission and wall-plug-efficiency from a

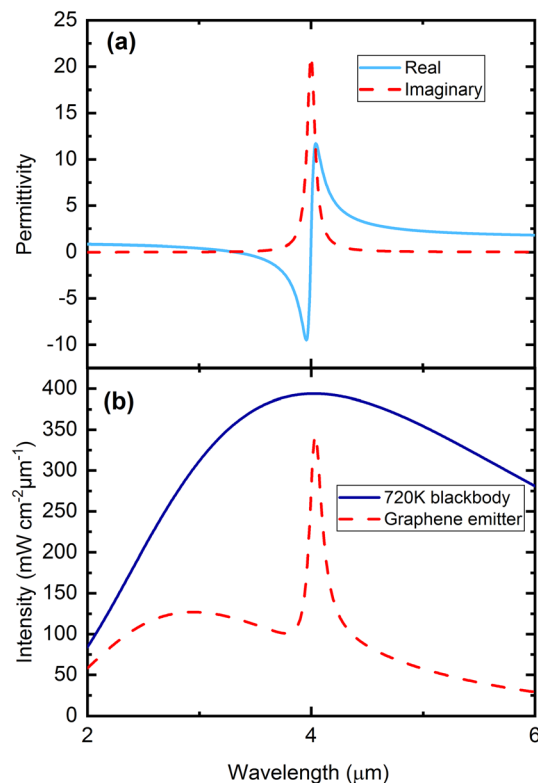


FIG. 4. (a) Calculated permittivity for the resonant layer. (b) The emission of a device with a resonant (red) compared to a 720K blackbody (blue line). Addition of the resonant layer creates a large, narrowband peak at the target wavelength, resulting in strong emission whose peak is close to the perfect blackbody.

device with a back reflector were approximately 300 mW/cm² and 0.07%, respectively. Such high relative efficiencies demonstrate the feasibility of developing a graphene based mid-infrared light emitting device, which could be more cost effective and sustainable to manufacture than either silicon MEMS or compound semiconductor based alternatives.

See the [supplementary material](#) for fits to the measured emission spectra using the second theoretical approach, which assumes the device is in thermal equilibrium.

The authors would like to thank Dr. Cheng Shi and Dr. Isaac Luxmoore for useful discussions. This work was funded via an EPSRC Fellowship (G.R.N.) in Frontier Manufacturing (Grant No. EP/J018651/1), the EPSRC Prosperity Partnership “The Tailored Electromagnetic and Materials Accelerator” (Grant No. EP/R004781/1), which is a collaboration with QinetiQ Ltd., and via the EPSRC Centre for Doctoral Training in Metamaterials (Grant No. EP/L015331/1).

AUTHOR DECLARATIONS

Conflict of Interest

The authors declare no competing interest.

Author Contributions

This manuscript was written through contributions of all authors. All authors have given approval to the final version of the manuscript.

DATA AVAILABILITY

The data that support the findings of this study are available from the corresponding author upon reasonable request.

REFERENCES

- See, for example, N. V. Zotova, N. D. Il'inskaya, S. A. Karandashev, B. A. Matveev, M. A. Remennyi, and N. M. Stus, “Flip-chip LEDs with deep mesa emitting at 4.2 μm ,” *Semiconductors* **40**, 697 (2006); M. K. Haigh, G. R. Nash, S. J. Smith, L. Buckle, M. T. Emeny, and T. Ashley, “Mid-infrared Al_xIn_{1-x}Sb light-emitting diodes,” *Appl. Phys. Lett.* **90**, 231116 (2007); G. R. Nash, H. L. Forman, S. J. Smith, P. B. Robinson, L. Buckle, S. D. Coomber, M. T. Emeny, N. T. Gordon, and T. Ashley, “Mid-infrared Al_xIn_{1-x}Sb light-emitting diodes and photodiodes for hydrocarbon sensing,” *IEEE Sens. J.* **9**, 1240 (2009); K. J. Cheetham, A. Krier, I. P. Marko, A. Aldukhayel, and S. J. Sweeney, “Direct evidence for suppression of Auger recombination in GaInAsSb/InAs mid-infrared light-emitting diodes,” *Appl. Phys. Lett.* **99**, 141110 (2011).
- B. I. Mirza, G. R. Nash, S. J. Smith, L. Buckle, S. D. Coomber, M. T. Emeny, and T. Ashley, “Recombination processes in midinfrared Al_xIn_{1-x}Sb light-emitting diodes,” *J. Appl. Phys.* **104**, 063113 (2008).
- I. J. Buss, M. J. Cryan, C. J. Railton, I. J. Craddock, G. R. Nash, and J. G. Rarity, “Finite-difference time-domain modeling of periodic and disordered surface gratings in AlInSb light emitting diodes,” *J. Lightwave Technol.* **28**, 1190 (2010).
- J. Abell, C. S. Kim, W. W. Bewley, C. D. Merritt, C. L. Canedy, I. Vurgaftman, J. R. Meyer, and M. Kim, “Interband cascade laser emitting at $\lambda = 3.75 \mu\text{m}$ in continuous wave above room temperature,” *Appl. Phys. Lett.* **92**, 191110 (2008).
- T. Inoue, M. D. Zoysa, T. Asano, and S. Noda, “Realization of dynamic thermal emission control,” *Nat. Mater.* **13**, 928–931 (2014).
- W. Li and S. Fan, “Nanophotonic control of thermal radiation for energy applications,” *Opt. Express* **26**, 15995–16021 (2018).
- D. G. Baranov, Y. Xiao, I. A. Nechepurenko, A. Krasnok, A. Alù, and M. A. Kats, “Nanophotonic engineering of far-field thermal emitters,” *Nat. Mater.* **18**, 920–930 (2019).
- A. Livingood, J. R. Nolen, T. G. Folland, L. Potechin, G. Lu, S. Criswell, J.-P. Maria, C. T. Shelton, E. Sachet, and J. D. Caldwell, “Filterless nondispersive infrared sensing using narrowband infrared emitting metamaterials,” *ACS Photonics* **8**, 472 (2021).
- S. S. Z. Ali, A. De Luca, R. Hopper, S. Boual, J. Gardner, and F. Udrea, “Low-power, low-cost infra-red emitter in CMOS technology,” *IEEE Sens. J. Electron Device Lett.* **15**, 6775 (2015), and references therein.
- A. Lochbaum, Y. Fedoryshyn, A. Dorodnyy, U. Koch, C. Hafner, and J. Leuthold, “On-chip narrowband thermal emitter for mid-IR optical gas sensing,” *ACS Photonics* **4**, 1371 (2017).
- L. Wojszwyk, A. Nguyen, A.-L. Coutrot, C. Zhang, B. Vest, and J.-J. Greffet, “An incandescent metasurface for quasimonochromatic polarized mid-wave infrared emission modulated beyond 10 MHz,” *Nat. Commun.* **12**, 1492 (2021).
- Y. D. Kim, H. Kim, Y. Cho *et al.*, “Bright visible-light emission from electrically biased suspended graphene,” *Nat. Nanotechnol.* **10**, 676–681 (2015).
- Y. D. Kim, Y. Gao, R.-J. Shiue *et al.*, “Ultrafast graphene light emitters,” *Nano Lett.* **18**, 934–940 (2018).
- Y. Miyoshi, Y. Fukazawa, Y. Amasaka, R. Reckmann, T. Yokoi, K. Ishida, K. Kawahara, H. Ago, and H. Maki, “High-speed and on-chip graphene blackbody emitters for optical communications by remote heat transfer,” *Nat. Commun.* **9**, 1279 (2018).
- S.-K. Son, M. Šiškins, C. Mullan *et al.*, “Graphene hot-electron light bulb: Incandescence from hBN-encapsulated graphene in air,” *2D Mater.* **5**, 011006 (2017).
- R.-J. Shiue, Y. D. Gao, C. Tan, C. Peng, J. Zheng, D. K. Efetov, Y. D. Kim, J. Hone, and D. Englund, “Thermal radiation control from hot graphene electrons coupled to a photonic crystal nanocavity,” *Nat. Commun.* **10**, 109 (2019).

- ¹⁷F. Luo, Y. Fan, G. Peng *et al.*, “Graphene thermal emitter with enhanced joule heating and localized light emission in air,” *ACS Photonics* **6**, 2117–2125 (2019).
- ¹⁸I. J. Luxmoore, C. Adlem, T. Poole, L. M. Lawton, N. H. Mahlmeister, and G. R. Nash, “Thermal emission from large area chemical vapor deposited graphene devices,” *Appl. Phys. Lett.* **103**, 131906 (2013).
- ¹⁹L. M. Lawton, N. H. Mahlmeister, I. J. Luxmoore, and G. R. Nash, “Prospective for graphene based thermal mid-infrared light emitting devices,” *AIP Adv.* **4**, 087139 (2014).
- ²⁰N. H. Mahlmeister, L. M. Lawton, I. J. Luxmoore, and G. R. Nash, “Modulation characteristics of graphene-based thermal emitters,” *Appl. Phys. Express* **9**, 012105 (2016).
- ²¹H. R. Barnard, E. Zossimova, N. H. Mahlmeister, L. M. Lawton, I. J. Luxmoore, and G. R. Nash, “Boron nitride encapsulated graphene infrared emitters,” *Appl. Phys. Lett.* **108**, 131110 (2016).
- ²²C. Shi, N. H. Mahlmeister, I. J. Luxmoore, and G. R. Nash, “Metamaterial-based graphene thermal emitter,” *Nano Res.* **11**, 3567–3573 (2018).
- ²³R. Kubo, “The fluctuation-dissipation theorem,” *Rep. Prog. Phys.* **29**, 255 (1966).
- ²⁴G. Kirchhoff, *J. Sci.* **20**, 130 (1860).
- ²⁵L. Novotny and B. Hecht, *Principles of Nano-Optics* (Cambridge University Press, 2006), Chap. 14, p. 454.
- ²⁶J.-J. Greffet, P. Bouchon, G. Brucoli, and F. Marquier, “Light emission by non-equilibrium bodies: Local Kirchoff law,” *Phys. Rev. X* **8**, 021008 (2018).
- ²⁷I. H. Baek, K. J. Ahn, B. J. Kang, S. Bae, B. H. Hong, D.-I. Yeom, K. Lee, Y. U. Jeong, and F. Rotermund, “Terahertz transmission and sheet conductivity of randomly stacked multi-layer graphene,” *Appl. Phys. Lett.* **102**, 191109 (2013).
- ²⁸T. Zhan, X. Shi, Y. Dai, X. Liu, and J. Zi, “Transfer matrix method for optics in graphene layers,” *J. Phys.: Condens. Matter* **25**, 215301 (2013).
- ²⁹M. N. Polyanskiy, see <https://refractiveindex.info> for “Refractive Index Database.”
- ³⁰P. Virtanen, R. Gommers, T. E. Oliphant *et al.*, “SciPy 1.0: Fundamental algorithms for scientific computing in Python,” *Nat. Methods* **17**, 261 (2020).
- ³¹M. C. Zheng, N. L. Aung, A. Basak, P. Q. Liu, X. Wang, J.-Y. Fan, M. Troccoli, and C. F. Gmachl, “High power spiral cavity quantum cascade superluminescent emitter,” *Opt. Express* **23**, 2713 (2015).
- ³²T.-Y. Chang, Y. Chen, D.-I. Luo *et al.*, “Black phosphorus mid-infrared light-emitting diodes integrated with silicon photonic waveguides,” *Nano Lett.* **20**, 6824–6830 (2020).
- ³³G. Brucoli, P. Bouchon, R. Häïdar, M. Besbes, H. Benisty, and J.-J. Greffet, “High efficiency quasi-monochromatic infrared emitter,” *Appl. Phys. Lett.* **104**, 081101 (2014).